RSC Applied Polymers

ROYAL SOCIETY OF CHEMISTRY

PAPER

View Article Online
View Journal | View Issue

Cite this: *RSC Appl. Polym.*, 2025, **3**, 469

Thiol–ene click reaction: a new pathway to hydrophilic metal–organic frameworks for water purification†

Mingyuan Fang,[a] Riansares Muñoz-Olivas,[b] Carmen Montoro *[c,d] and Mona Semsarilar *[a]

Post-synthetic modification (PSM) is a useful strategy to introduce new functional groups to metal–organic framework (MOF) structures in order to tune their properties for different applications. One of the methodologies used for PSM of MOFs is click chemistry known for their high reaction efficiency and good compatibility with various functional groups. Herein, we report the first PSM example of a thiol-functionalized MOF. Pores surface of the Zr-MSA MOF (based on Zr and mercaptosuccinic acid (MSA)) was decorated with short poly (ethylene glycol) (PEG) chains using click chemistry. Mono or di acrylate functional PEG were attached to the MOF pore walls either using UV irradiated thiol–ene click or Michael addition thiol–ene click reactions. The use of mono-functionalized PEG resulted in the formation of colloidal stable particles while the use of di-functionalized PEG led to a cross-linked network. The properties of PEG modified Zr-MSA were fully characterized using various structural, textural and morphological techniques. The sample containing the highest PEG content was then used for the removal of mercury, Hg(II); chromium, Cr(VI) and rhodamine B (RhB) from water. Results suggest that the hybrid material was able to capture these pollutants while maintaining a good colloidal stability and hydrophilicity. Therefore, click chemistry has been proved as an efficient strategy for the surface modification of MOF particles with low molecular weight polymers.

Received 15th November 2024,
Accepted 14th February 2025

DOI: 10.1039/d4lp00341a

rsc.li/rscapplpolym

1. Introduction

Metal–organic frameworks (MOFs) are crystalline porous materials built from metal ions interconnected through organic ligands, giving rise to an ordered structure of channels and cavities accessible to guest molecules.[1] In comparison with other classical porous materials, such as zeolites and active carbon, the main advantage of MOFs lies in the rational design of their structures.[2] This can be attributed to several reasons: (i) the synthesis of MOFs is usually carried out under controlled experimental conditions; (ii) there is an infinite number of combinations of organic ligands with metal ions; (iii) a certain combination of a rigid organic ligand and a metal with the appropriate coordination geometry always produces a specific framework. The reticular synthesis approach allows tuning the structures and properties of MOFs without changing the connectivity or topology through two different routes: direct synthesis[3,4] and post-synthetic modification (PSM) of ligands and/or metal clusters. Then, they can be designed for specific applications, such as gas storage and separation,[5–7] liquid separation,[8] heterogeneous catalysis,[9,10] drug delivery,[11,12] among others.[13] PSM is often the strategy of choice for introducing new functional groups to the already prepared MOF structures.[14–17] One of the main strategies used in PSM of MOFs is based on click chemistry since it shows high reaction efficiency and good compatibility with various functional groups.[18–20] Azide–alkyne and thiol–ene click reactions have been extensively used to modify and functionalize materials in an efficient manner.[21–23] Modification of MOFs using azide–alkyne click reaction has been previously reported.[18,24] However, thiol–ene click reaction has not been used much for the modification of MOFs despite being a simple, robust, and efficient reaction in the formation of S–C bonds under relatively facile

[a]*Institut Européen des Membranes—IEM UMR 5635, Univ Montpellier, CNRS, ENSCM, 34090 Montpellier, France. E-mail: mona.semsarilar@umontpellier.fr*
[b]*Departamento de Química Analítica, Universidad Complutense de Madrid, Ciudad Universitaria, 28040 Madrid, Spain*
[c]*Departamento de Química Inorgánica, Universidad Autónoma de Madrid, 28049 Madrid, Spain. E-mail: carmen.montoro@uam.es*
[d]*Institute for Advanced Research in Chemical Sciences (IAdChem), Universidad Autónoma de Madrid, 28049 Madrid, Spain*

†Electronic supplementary information (ESI) available: Experiment summary, TEM, SEM, optical images, table of PEG clicked amount and ^{1}H NMR spectrum of modified Zr-MSA after HF digestion. See DOI: https://doi.org/10.1039/d4lp00341a

conditions. Rieger *et al.*[25] prepared an olefin-tagged 4,4′-bipyridine linker (L^1) that was used to synthesize Zn-TDC (TDC = 9,10-triptycenedicarboxylate) paddle-wheel MOF [Zn_2 $(TDC)_2L^1$]. The thiol–ene click PSM of [Zn_2 $(TDC)_2L^1$] was then synthesized by ethanethiol under UV irradiation. A similar strategy was used by Wang *et al.*[26] where an allyl functionalized UiO-68 (synthesized using triphenyl-4,4′-dicarboxylic acid (TPDC) linker through a multi-step protocol) was modified *via* thiol–ene click performed under UV in the presence of 2,2-dimethoxy-2-phenylacetophenone photo-initiator. Later, the same group prepared UiO-68-An/Ma (anthracene/maleimide) through the multivariate approach by mixing two linkers and functionalizing the maleimide groups using Diels–Alder and thiol–ene reactions to tune the electron-accepting ability of the UiO-68.[27] Recently, PSM of MOFs *via* thiol–ene click was performed in aqueous media in the presence of 2-mercaptoethanol at room temperature. Yameen *et al.*[28] performed a PSM of IRMOF-3-Zn using NH_2-1,4-benzenedicarboxylic acid as the linker. At first, 4-maleimidobutyroyl chloride was grafted to the amine groups to obtain the maleimide-tagged IRMOF-3-Zn. Then, cysteine was used as the thiol to click with the maleimide catalyzed by triethylamine at ambient conditions. Similarly, Queen *et al.*,[29] used Michael addition to click 1*H*,1*H*,2*H*,2*H*-perfluorodecanethiol on a series of dopamine modified MOFs (HKUST-1 (Cu), ZIF-67 (Co), ZIF-8 (Zn), UiO-66 (Zr), Cu-TDPAT (Cu, 2,4,6-tris(3,5-dicarboxylphenylamino)-1,3,5-triazine)) to increase their stability. Cheng *et al.*[30] prepared Zr (Hf)-UiO-66 with thiol functions by using 2,5-dimercapto-1,4-benzenedicarboxylic acid (H_2DMBD) linker. Then, 1*H*,1*H*,2*H*-perfluoro-1-decene and 1*H*,1*H*,2*H*-perfluoro-1-hexene was attached to the MOF under UV irradiation with the photoinitiator (2-hydroxy-2-methyl propiophenone).[31]

The majority of the examples in the literature require multi-step reactions and purification steps in order to add the specific functionalities required for the click reaction. To date, only one example of a thiol–ene click on a thiol-functionalized MOF has been reported.[30] And to the best of our knowledge, there is no report on clicking a polymer chain to a thiol-functionalized MOF.

Herein, a thiol-functionalized MOF, Zr-MSA,[32] was modified using two pathways; UV irradiated thiol–ene click and Michael addition (Scheme 1). Two poly (ethylene glycol) acrylates, (monofunctional PEG-acrylate-480 and difunctional PEG-acrylate-575) were chosen as the model polymers for the surface modification of the Zr-MSA *via* click reactions. The attachment of the soluble PEG chains on the MOF surface would render colloidal stability to the MOF structure. Moreover, the use of difunctional PEG chains could act as a cross-linker and fix the MOF structure in a polymer network/matrix. Analogous approaches have been carried out for the preparation of hybrid membranes using thiol–ene click reactions, which favor the integration of the MOF into the internal structure of the membrane without compromising its physical properties.[33,34] In this regard, our methodology enables the material to be easily obtained in gel form without the need for any polymeric matrix that would reduce the MOF's efficiency. On the other hand, PEG is a hydrophilic and biocompatible polymer, which is one of the most used polymers in biomedical and environmental applications.[35,36] PEG is often employed to improve the hydrophilicity and enhances the surface functionality of different materials.[37,38] The thiol–ene click reactions including UV irradiated click and the Michael addition are usually performed under mild conditions: room temperature, air atmosphere, low amount of photo-initiator or catalyst and wide choice of solvents. Both reactions are efficient with high yields. Moreover, in the thiol Michael addition pathway the use of nucleophile catalyst reduces the chance of radical coupling reactions that often happen in the UV irradiated thiol–ene click.[39] Hence, these two strategies are ideal for PSM of MOFs.

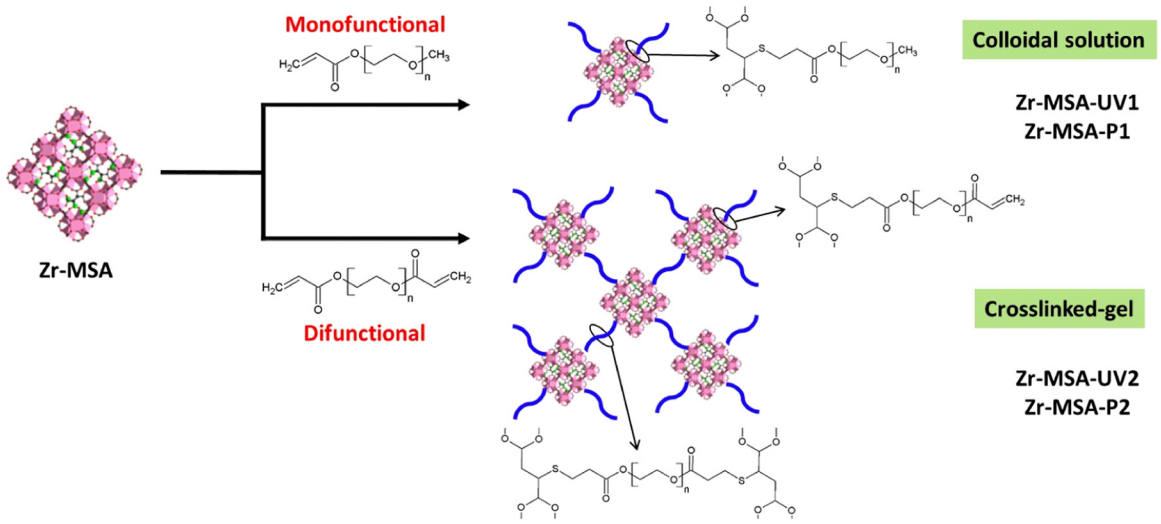

Scheme 1 PSM *via* thiol–ene click reactions used for the modification of Zr-MSA with PEG acrylates.

The resulting MOF-polymers were fully characterized. The capacity of these novel structures for pollutant removal such as Hg(II), Cr(VI) and rhodamine B (RhB) were evaluated.

2. Experimental section

2.1. Materials

Zirconium(IV) chloride ($ZrCl_4$; ≥99.5% trace metals basis), mercaptosuccinic acid (MSA; 97%), poly (ethylene glycol) methyl ether acrylate with average M_n = 480 (PEG-acrylate-480; BHT and MEHQ used as inhibitor), poly (ethylene glycol) diacrylate with average M_n = 575 (PEG-diacrylate-575; MEHQ as inhibitor), 2,2-dimethoxy-2-phenylacetophenone (DMPAP; 99%), *N*,*N*-dimethylformamide (DMF), tributylphosphine, (TBP; 97%), rhodamine B (RhB; ≥95%), and hydrochloric acid (HCl; 37%) were purchased from Sigma-Aldrich. Potassium dichromate ($K_2Cr_2O_7$; analytical grade) was purchased from Carlo Erba. Hydrofluoric acid (HF; 40%) and was purchased from Prolabo. Mercury chloride ($HgCl_2$) was an ICP/MS Agilent standard 1000 mg L^{-1} solution. Solvents were purchased from Fisher Scientific and VWR. All the reagents were used without further purification.

2.2. Synthesis of Zr-MSA

Zr-MSA was prepared following the procedure reported previously by Gu *et al.*[32] Briefly, 233 mg of $ZrCl_4$, 150 mg of MSA and 160 μL of formic acid (FA) were dissolved in 2 mL of water. After ultrasonic treatment for 1 min, the mixture was kept in an oven at 80 °C for 2 h. The solid was then washed with water (20 mL) and ethanol (EtOH, 2 × 10 mL). Finally, the sample (about 250 mg) was dried at 80 °C for 12 h in a vacuum oven.

2.3. UV irradiated click reaction

Modification of Zr-MSA with monofunctional PEG (Zr-MSA-UV1). 100 mg of Zr-MSA was activated at 80 °C and charged with 1 mL of DMF, 120 μL of PEG-acrylate-480 and 150 mg of DMPAP photoinitiator. The reaction was irradiated under UV light (365 nm) for 12 h. The resulting white suspension was centrifuged and rinsed with acetone (2 × 5 mL) and EtOH (3 × 5 mL). 105 mg of white powder was obtained after 12 h of drying under vacuum at 60 °C.

Modification of Zr-MSA with difunctional PEG (Zr-MSA-UV2). 100 mg of Zr-MSA was activated at 80 °C and charged with 1 mL of DMF, 150 μL of PEG-diacrylate-575 and 150 mg of DMPAP photoinitiator. The reaction was irradiated under UV light (365 nm) for 12 h. The resulting white gel was rinsed with acetone (2 × 5 mL) and EtOH (3 × 5 mL). After drying at 60 °C for 12 h under vacuum, 118 mg of white solid was isolated.

2.4. Phosphine catalyzed Michael addition click reaction

Modification of Zr-MSA with monofunctional PEG (Zr-MSA-P1). 100 mg of Zr-MSA was activated at 80 °C before being placed in a glass tube, which was then charged with 1 mL of DMF, 120 μL of PEG-acrylate-480 and TBP (4 μL, adding as 2 vol% solution in DMF). The final mixture was reacted under magnetic stirring at room temperature for 24 h. The resulting white suspension was centrifuged and then rinsed with acetone (2 × 5 mL) and EtOH (3 × 5 mL). After 12 h of vacuum drying at 60 °C, 73 mg of white powder was obtained.

Modification of Zr-MSA with difunctional PEG (Zr-MSA-P2). 100 mg of Zr-MSA was activated at 80 °C before being placed in a glass tube, which was then charged with 1 mL of DMF, 150 μL of PEG-diacrylate-575 and TBP (4 μL, adding as 2 vol% solution in DMF). The final mixture was reacted under magnetic stirring at room temperature for 24 h. The resulting white suspension was centrifuged and then rinsed with acetone (2 × 5 mL) and with EtOH (3 × 5 mL). After 12 h of vacuum drying at 60 °C, 92 mg of white powder was obtained.

2.5. Hg(II) capture

In a typical adsorption experiment, a sample of Zr-MSA-UV2 gel (10 mg) was placed in a porous frit cartridge and emerged into 1 mL aqueous solution (pH of 5.5) of $HgCl_2$ with a concentration of 10 mg L^{-1}. Then, the solution was stirred at ambient temperature (around 24 °C) using a Vortex system and filtered under vacuum. Hg(II) concentrations in the filtrated solutions were determined using a Varian SpectrAA 55 B Atomic Absorption Spectrometry provided with a Cold Vapor Unit, which is, a typical methodology applied for trace analysis of mercury.[40] Absorbance measured at 254 nm is proportional to the mercury content in the sample. This protocol was carried out at different pH values (from 1–10) to assess the influence of this parameter in Hg(II) capture. Additionally, adsorption kinetics, adsorption isotherms, polymer reusability and selectivity test were studied.

The affinity for Hg(II) was estimated by measuring the distribution coefficient (K_d), defined as:

$$K_d = \frac{(C_i - C_f)}{C_f} \times \frac{V}{m} \quad (1)$$

where C_i (mg g^{-1}) is the initial metal ion concentration, C_f (mg g^{-1}) is the final equilibrium metal ion concentration, V (mL) is the volume of the treated solution and m (g) is the mass of the adsorbent used.

The kinetics of mercury removal from water was also evaluated. Different kinetic models have been developed to describe the kinetics of heavy metal removal.[41–43] In this case, the data are better fitted to the pseudo-second order model, expressed as:

$$\frac{t}{q_t} = \frac{1}{K_2 q_e^2} + \frac{t}{q_e} \quad (2)$$

where K_2 (g mg^{-1} min^{-1}) is the rate constant of pseudo-second order adsorption, q_t (mg g^{-1}) is the amount of Hg(II) adsorbed at time t (min), and q_e (mg g^{-1}) is the amount of Hg(II) adsorbed at equilibrium.

2.6. Cr(VI) and RhB capture

Cr(VI) and RhB adsorption experiments were carried out using 10 mL solution of RhB (C_0 = 2.1 × 10^{-5} mol L^{-1}) and $K_2Cr_2O_7$ (C_0 = 3.6 × 10^{-3} mol L^{-1}). 100 mg of Zr-MSA-UV2 gel were added into the Cr(VI) or RhB solution at room temperature without stirring. The concentrations of Cr(VI) and RhB in solution as a function of time were determined using a UV spectrometer (SHIMADZU UV-2401PC spectrophotometer) at 554 nm and 257 nm, respectively.[44,45] The regeneration of the Zr-MSA-UV2 gel for the RhB removal was performed *via* washing with water (2 × 10 mL) and EtOH (3 × 10 mL). Then, the samples were dried under vacuum at 80 °C. The percentage of Cr(VI) and RhB removal were calculated using eqn (3):

$$R = \frac{(C_0 - C_f)}{C_0} \times 100\% \quad (3)$$

where C_0 (mg g^{-1}) is the initial concentration, C_f (mg g^{-1}) is the final equilibrium concentration.

2.7. Characterization

Powder X-ray diffraction (PXRD) measurements were performed on a X'pert Pro (PAN Analytical) X-Ray diffractometer in reflectance parallel beam/parallel slit alignment geometry. The measurement employed Cu Kα line focused radiation at 800 W (40 kV, 20 mA) power. Samples were observed using a 0.017° 2θ step scan from 5° to 50° with an exposure time of 120 s per step. Fourier-transform infrared (FT-IR) spectra were performed on a Thermo Nicolet iS50 FT-IR spectrometer in transmission mode. Each sample was applied 32 scanning from 400 cm^{-1} to 4000 cm^{-1}. ^{1}H NMR spectra were recorded at room temperature on a Bruker Avance spectrometer 400 MHz. Thermogravimetric analysis (TGA) was performed with TA Instruments SDT Q600 by heating the sample to 1000 °C under nitrogen flux (100 mL min^{-1}) at a heating rate of 10 °C min^{-1}. Scanning Electron Microscopy (SEM) images were observed under Hitachi S4800 with 0.1–30 kV working voltage. Membrane's cross-section samples were prepared by quickly breaking the membrane under liquid nitrogen. Transmission Electron Microscopy (TEM) images were obtained from JEOL 1200 EXII (or JEOL 1400) under working voltage up to 120 kV. TEM samples were prepared by placing 10 μL of the sample (100 times dilution of reaction mixture) on a carbon-coated copper grid for 60 s. Then, the grid was dried under ambient conditions. Nitrogen adsorption isotherms were measured at 77 K on a Micromeritics ASAP 2020 Plus Adsorption Analyzer. Prior to measurement, powder samples were degassed for 12 h at 80 °C.

3. Results and discussion

3.1. Synthesis and characterization of the materials

Zr-MSA was synthesized through a green route with a structure similar to the well-known UiO-66.[32] This MOF has reactive alkyl thiol groups, an excellent chemical stability, relatively large pore and small particle size.[32,46] Surface of this synthesized Zr-MSA was then modified with a mono- (PEG-acrylate-480) and di-PEG acrylates (PEG-diacrylate-575) employing UV irradiated and Michael addition thiol–ene click reactions. These relatively short PEG chains were selected to ensure good chain end fidelity (achieving a high yield of the click reaction) and to add sufficient softness to the MOF particles avoiding the risk of long polymer chains hindering the accessibility of the MOF active sites. The resulting structures are labelled as Zr-MSA-UV1, Zr-MSA-UV2, Zr-MSA-P1 and Zr-MSA-P2 (Scheme 1). These samples were all suspensions apart from Zr-MSA-UV2 that was a gel. All four samples were fully characterized.

PXRD patterns of the obtained Zr-MSA after click reactions (Fig. 1) exhibit similar Bragg diffraction peaks of the pristine Zr-MSA, indicating that the modification with PEG functionalities does not affect the topology nor the crystallinity.[32]

The characteristic vibrational bands of the modified Zr-MSA were identified by FT-IR spectroscopy. As shown in Fig. 2a and b, a new broad band at about 2950 cm^{-1} appeared which contribute to the C–H stretching from the PEG chain. The intensity of the broad band approximately at 2500 cm^{-1} which is the S–H vibration, was reduced for all 4 samples after the click reactions confirming that the thiol groups of the Zr-MSA were partially consumed. The intense band at 1725 cm^{-1}, indicating the C=O stretching of the acrylate group shifted to 1660 cm^{-1} after the click reactions. This suggests the coupling between the thiol functionality of the Zr-MSA and the vinyl moiety of the PEG-acrylate, forming S–C bonds. In the Zr-MSA-UV2 sample, the C=O stretching band of the acrylate group at 1725 cm^{-1} (Fig. 2b) is still visible but less intense.

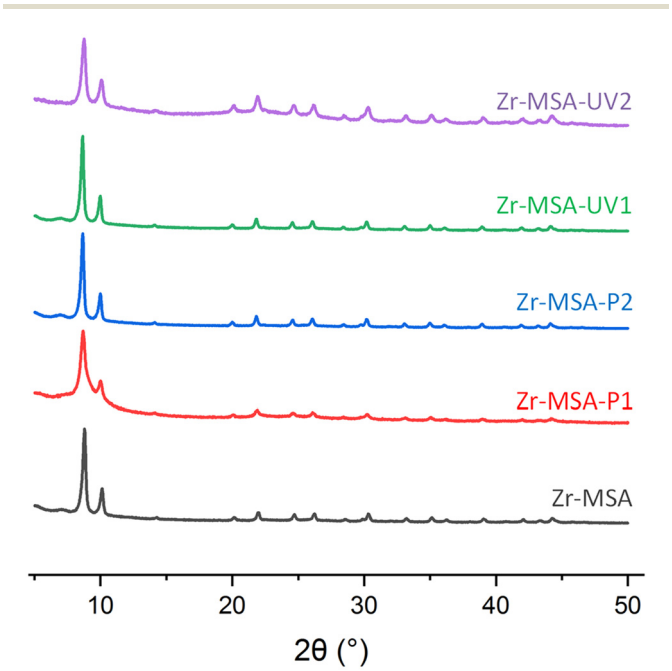

Fig. 1 XRD patterns of Zr-MSA, Zr-MSA-UV1, Zr-MSA-UV2, Zr-MSA-P1 and Zr-MSA-P2.

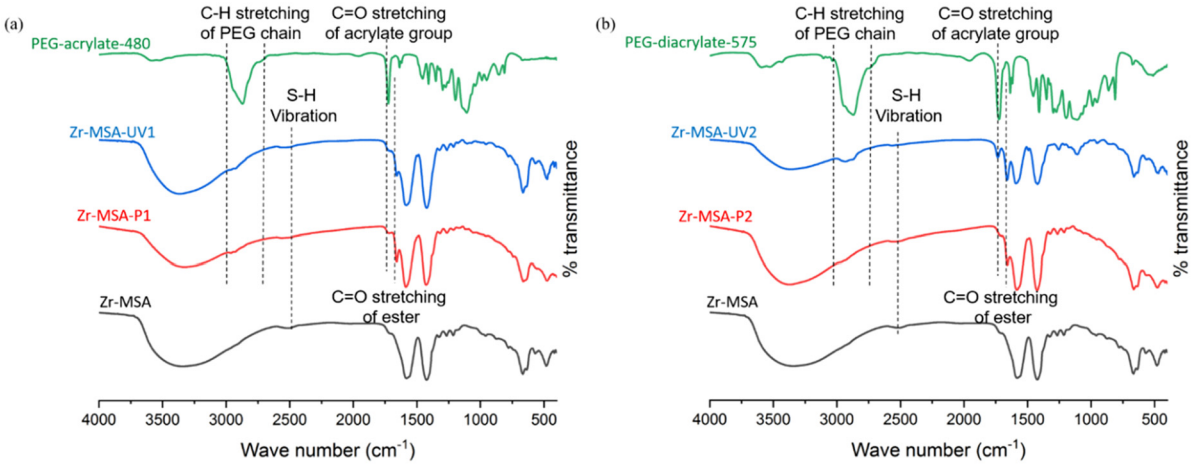

Fig. 2 FT-IR measurements of (a) PEG-acrylate-480, Zr-MSA-UV1, Zr-MSA-P1 and Zr-MSA; (b) PEG-diacrylate-575, Zr-MSA-UV2, Zr-MSA-P2 and Zr-MSA.

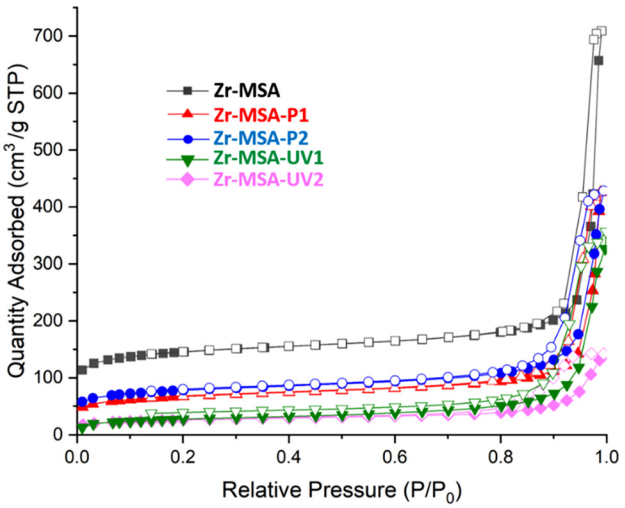

Fig. 3 N_2 adsorption–desorption isotherms measured at 77 K for pristine Zr-MSA, Zr-MSA-UV1, Zr-MSA-UV2, Zr-MSA-P1 and Zr-MSA-P2. Filled and empty symbols represent adsorption and desorption processes, respectively.

This could either be because the PEG-diacrylate only reacted on one side with the SH on Zr-MSA (leaving an unreacted vinyl bond) or because some unreacted PEG-diacrylate are trapped inside the Zr-MSA-UV2 gel structure.

Nitrogen adsorption isotherms were used to measure the porosity of the modified Zr-MSA structures (Fig. 3). The BET surface area of Zr-MSA was about 550 $m^2\ g^{-1}$. However, as expected, the surface areas as well as the pore volume of the modified Zr-MSA were reduced (see Table S2†). The obtained surface areas were 232 $m^2\ g^{-1}$, 269 $m^2\ g^{-1}$, 97 $m^2\ g^{-1}$ and 90 $m^2\ g^{-1}$ for Zr-MSA-P1, Zr-MSA-P2, Zr-MSA-UV1 and Zr-MSA-UV2, respectively. This decrease in the surface area corresponds to the presence of the PEG chains which reduce the pore accessibility. The decrease of UV modified (Zr-MSA-UV1 and Zr-MSA-UV2) was more noticeable than Michael addition modification samples. This result could be due to the higher yield of the UV click reaction resulting in more PEG chains getting grafted to the Zr-MSA surface. It should also be noted that the PEG chains become more rigid at the nitrogen adsorption temperature test (77 K). This loss of flexibility could prevent the diffusion of water or solvent molecules leading to lower adsorption capacity. In contrast, at room temperature, the flexible PEG chains facilitate the diffusion of molecules inside the porous structure of the Zr-MSA. For example, when the water uptake of the least porous sample (Zr-MSA-UV2) was tested at room temperature, water uptake of 136 wt% was achieved, confirming the accessibility of the pores under ambient conditions.

The TGA profiles (Fig. 4a) of Zr-MSA and Zr-MSA-UV1 have very similar weight loss. Below 100 °C, the weight loss of Zr-MSA-UV1 is higher due to the extra water molecules retained in the hydrophilic PEG chains. The next degradation step is when the MOF ligands and PEG chains gradually decompose and reach a stable plateau at around 650 °C. The final residue of Zr-MSA-UV1 was 2 wt% less than that of Zr-MSA, representing the weight percentage of the PEG chains clicked to the Zr-MSA framework.

In contrast, Zr-MSA-UV2 (Fig. 4a) has a very different thermal behavior compared to the non-modified Zr-MSA. Like Zr-MSA-UV1, the weight loss of Zr-MSA-UV2 was higher than Zr-MSA due to the presence of the hydrophilic PEG chains. Then, from 100 to 250 °C, the weight loss of Zr-MSA-UV2 slowed down. This could indicate that the PEG-chains have covered the surface of Zr-MSA crystals protecting them from rapid decomposition. When the temperature was gradually increased to 400 °C, PEG chains started to decompose as well as the organic linker of the Zr-MSA. Finally, the Zr-MSA-UV2 showed 23% more weight loss than Zr-MSA, representing the weight percentage of the PEG chains attached onto the Zr-MSA framework.

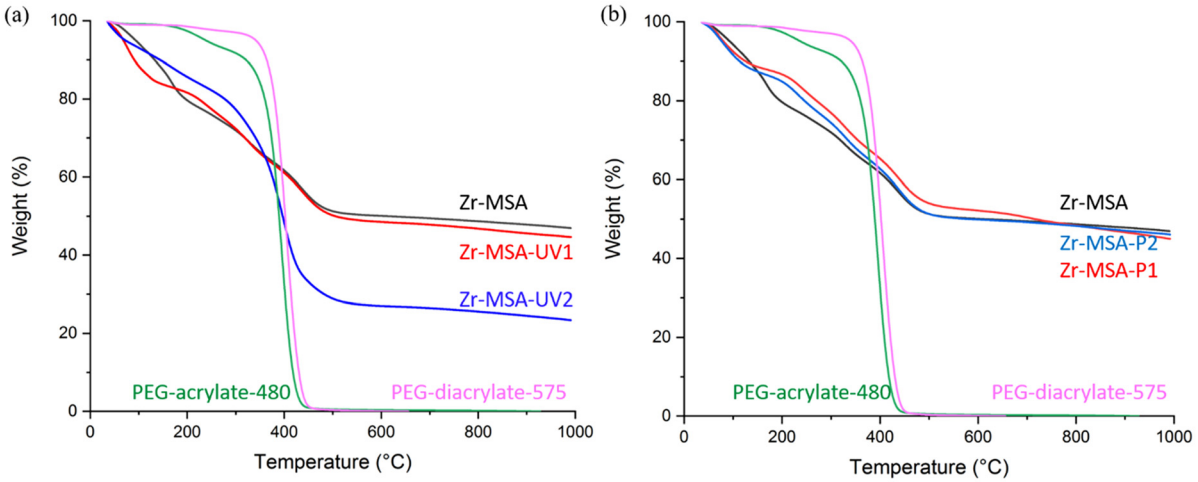

Fig. 4 TGA of (a) Zr-MSA, PEG-acylate-480, PEG-diacrylate-575, Zr-MSA-UV1 and Zr-MSA-UV2; (b) Zr-MSA, PEG-acylate-480, PEG-diacrylate-575, Zr-MSA-P1 and Zr-MSA-P2.

The TGA profiles of the Zr-MSA, Zr-MSA-P1 and Zr-MSA-P2 (Fig. 4b) showed similar weight loss steps. At the region below 100 °C, the weight loss of Zr-MSA-P1 was higher due to the hydrophilic PEG chains trapping more water molecules in the sample. Then the Zr-MSA ligands and PEG chains gradually decompose to reach a stable plateau at around 800 °C. The difference between the amount of the final residue in Zr-MSA and Zr-MSA-P1/P2 was almost the same (within about 0.5 wt%), representing the weight percentage of the attached PEG chains.

By comparing the final weight loss of Zr-MSA-P1 and Zr-MSA-UV1, weight percentage of PEG-acrylate-480 presented in Zr-MSA-UV1 is slightly higher than Zr-MSA-P1. It seems that the click reaction under UV irradiation is more efficient than the Michael addition catalyzed by phosphine. In contrast, the final weight loss of Zr-MSA-UV2 is much higher than Zr-MSA-P2. This difference might be related to a side reaction where the difunctional PEG chains polymerize together (cross-link) under UV irradiation. While such side reaction could not take place under phosphine catalyzed Michael addition.

To further confirm the quantity of the PEG chains clicked onto the Zr-MSA, the modified MOFs were digested and analyzed by ^{1}H NMR. The results indicated that the amount of PEG clicked onto the Zr-MSA-UV1 was around 3.8 wt% and 7.3 wt% for Zr-MSA-UV2. These values are higher than those obtained for the samples modified *via* Michael addition. The calculated amount of the clicked PEG chains onto the Zr-MSA-P1 was about 2.9 wt% (Table S3 and Fig. S1†).

TEM image of Zr-MSA before modification (Fig. S2†) showed particle size in the range of 25 to 50 nm and, particles tend to form aggregates. However, after the modification with the PEG chains, less aggregates were visible. In Fig. 5a and c (Zr-MSA-UV1 and Zr-MSA-P1) mainly individual particles could be seen of a similar size than Zr-MSA (25 to 50 nm). This observation is surely related to the presence of the polymer chains on the outer surface of the Zr-MSA, bringing about better interaction with the solvent, long-term colloidal stability and subsiding the particle aggregation. In addition, similar results were observed in SEM images (Fig. S3a, b and d†). Zr-MSA-UV2 particles are bundled (Fig. 5b inset) perhaps due to the presence of the cross-linked PEG chains as explained previously. Zr-MSA-P2 (Fig. 5d), presented particle sizes of 25 to 50 nm, which are analogous with the size obtained for Zr-MSA and, individual particles with a film of polymer visible in the background, indicating the presence of the cross-linked difunctional PEG chains (Fig. S3e†). In SEM images of Zr-MSA-UV2, connected crystallites could be observed (Fig. S3c†).

3.2. Adsorption capability of the materials

In order to evaluate the applicability of the PEG-modified Zr-MSA MOFs, the Zr-MSA-UV2 sample was selected due to the described physical properties as user-friendly solid sorbent. Hg(II), Cr(VI) and rhodamine B (RhB) were tested as model water contaminants.

Considering the strong affinity between alkyl thiol and Hg(II) ions, Zr-MSA has already been used for capturing Hg(II).[46] However, our approach presents the advantage of improving the processability of the powder Zr-MSA since the presence of the PEG chains lead to formation of a stable solid sorbent (rather than the crystalline MOF powder). The capability of Zr-MSA-UV2 to capture Hg(II) ions from water was measured by placing 10 mg of this material in a 10 mg L^{-1} aqueous solution of $HgCl_2$. The isotherm absorption data obtained for this sample fitted well with the Langmuir model giving a correlation coefficient of 1 (Figure S4†). The maximum absorption capacity was 40.21 mg g^{-1}, with this value being lower than for pristine Zr-MSA due to the lower number of available –SH groups in the modified Zr-MSA. The removal efficiency was determined *via* absorption kinetic studies. As it can be seen in Fig. 6, the absorption of Hg(II) showed a fast kinetic where the Hg(II) was absorbed in less than 5 minutes. This is due to the presence of hydrophilic PEG chains on the MOF surface that

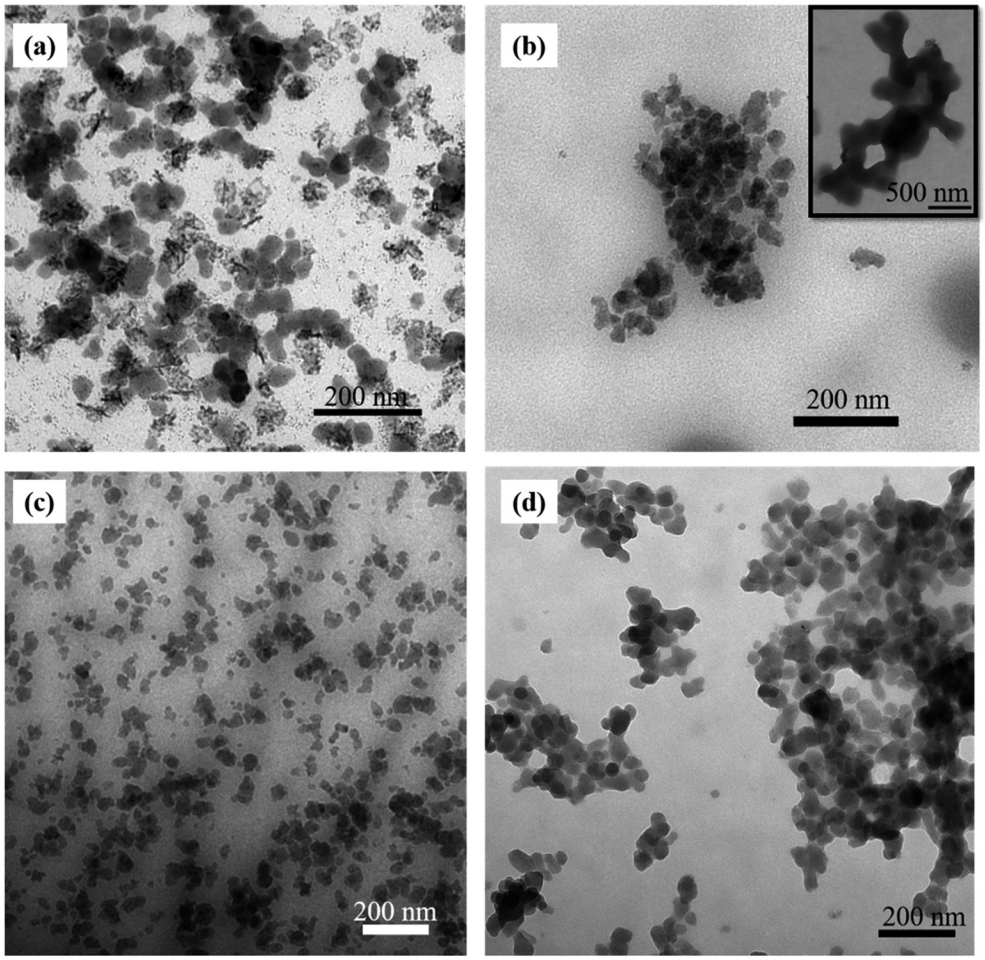

Fig. 5 TEM images of (a) Zr-MSA-UV1, (b) Zr-MSA-UV2, (c) Zr-MSA-P1 and (d) Zr-MSA-P2.

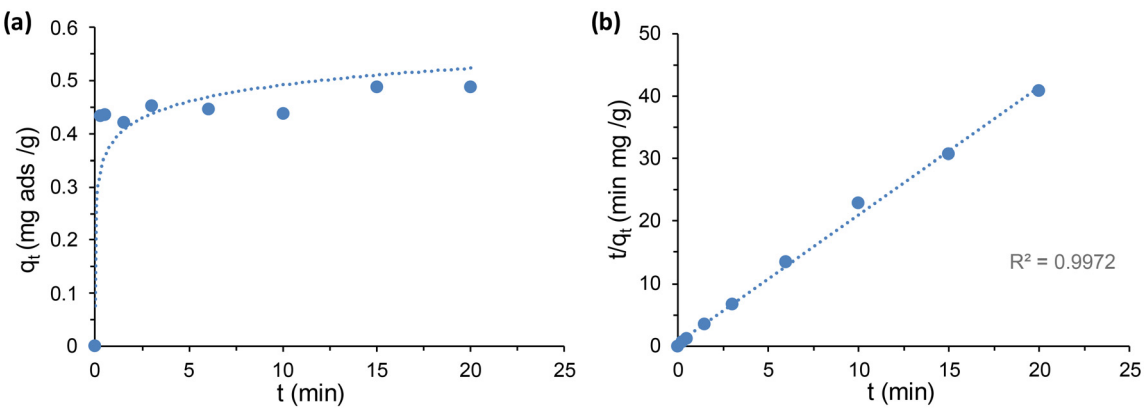

Fig. 6 (a) Hg(II) absorption kinetics of Zr-MSA-UV2 for 20 minutes contact. (b) The pseudo-second-order kinetic plot for the absorption (Hg(II) concentration of 10 mg L^{-1}).

helps water diffusion and absorption of Hg(II) in comparison to the Zr-MSA powder. The kinetic data fitted well to a pseudo second-order model, with a K_2 coefficient of 9.024 g mg^{-1} min^{-1}, perfectly comparable to the Zr-MSA (K_2 coefficient of 15.33 g mg^{-1} min^{-1}).[44]

The absorbent's affinity for Hg(II) at 5 minutes was estimated by the K_d measurement reaching a value of 6.6×10^6 mL g^{-1} in water with an initial Hg(II) concentration of 10 mg L^{-1}. Under these conditions, the removal efficiency was 99% (initial load of 10 000 ng in 10 mg of Zr-MSA-UV2 reduced to a

final amount of 0.2 ng). This indicates a decrease from the initial concentration of 10 mg L^{-1} to a final concentration of 0.15 μg L^{-1}. Changing pH from 2 to 7.5 did not affect the Hg (II) absorption capacity (Fig. S5†), meaning that the material can be used for different type of contaminated water bodies (natural waters, industrial effluents, wastewater, *etc.*). Additionally, Zr-MSA-UV2 could be regenerated by desorbing the captured Hg(II) with HCl solutions and re-used for at least 3 cycles without any loss of absorption capacity. An important factor to be considered when evaluating the absorption capacity of the material is the interference of other metal ions that can be present in the studied waters. The selectivity of the material for Hg(II) absorption was evaluated in the presence of other metal ions. For this, tap water, seawater and industrial wastewater samples were employed. The Hg(II) content in these samples were really low, 0.40 μg L^{-1}. Then, these water samples were doped with 50 μg L^{-1} of Hg(II). In all cases, 95% Hg(II) removal was obtained indicating that the water matrix did not cause a significant interference in Hg(II) removal.

The next contaminant tested was Cr(VI). Previously, it was shown that Zr-MSA could absorb and degrade the toxic Cr(VI) *via* coordination of the metal with the thiol and thiolester groups.[32,47,48] $K_2Cr_2O_7$ salt was chosen here in order to confirm the availability of the remaining non-reacted thiol and thioether functionalities after grafting the PEG chains. The chromate Cr(VI) absorption from a relatively high concentration (100 mg L^{-1}) at pH 3 (Fig. 7), was more than 50% after 1 hour and close to 90% after 22 hours. The concentration of Cr(VI) decreased rapidly and the color of the Zr-MSA-UV2 changed from white to brown and then gradually turned to emerald green, indicating the absorption and degradation of Cr(VI) to Cr(III) (Fig. S6c†). The Cr(VI) absorption and degradation results, confirms that some free thiol groups were still available in the structure of the Zr-MSA-UV2 after the click reaction since it could still absorb the toxic Cr(VI) and reduce it to Cr(III) through the thiol groups.

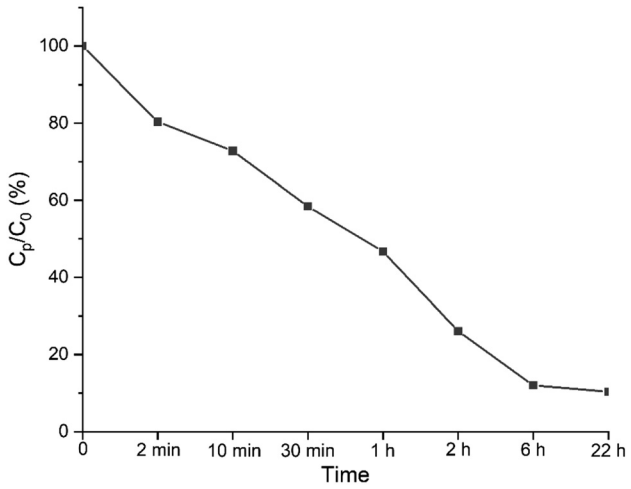

Fig. 7 Absorption of Cr(VI) on Zr-MSA-UV2 at pH3.

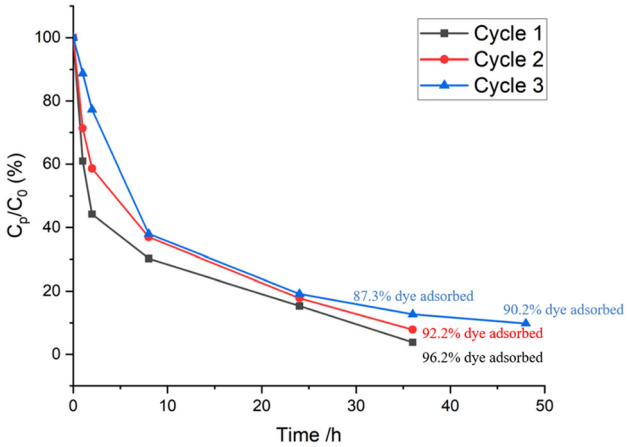

Fig. 8 Adsorption of RhB on Zr-MSA-UV2 at different cycles.

Finally, the material was tested for the removal of RhB from water. This is a commonly used cationic dye with relatively high molecular weight (479 g mol^{-1}). The adsorption of RhB showed that more than 90% of RhB was adsorbed on the Zr-MSA-UV2 even after three adsorption/desorption cycles (Fig. 8) from the dye solution with an initial concentration of 2.1 × 10^{-5} mol L^{-1}. This suggests that the PEG modified Zr-MSA has enough accessible pores to uptake the relatively large RhB molecule. In addition, it is very easy to handle the PEG modified MOF as compared to the initial Zr-MSA powder (Fig. S6a and b†). This physical aspect allows facile removal of the material from solution without the need for centrifugation, addition of flocculating agents or any other extra steps. Furthermore, the PEG modified Zr-MSA could be regenerated and re-used after washing and drying.

The results from the adsorption studies of Hg(II), Cr(VI) and RhB highlight the synthesized material's applicability for removing water pollutants. When comparing the obtained results with those reported for MOF/hydrogel composite adsorbents for the removal of metal ions,[49] organic dyes, and drug residue molecules found in the literature[50,51] it can be stated that, the synthesized adsorbent is performant as it maintains more than 90% efficiency after several adsorption/desorption cycles. Its capacity for removal of Cr(VI) is very similar to reported MOFs@Abs[52] as well as improved results for the adsorption of RhB when compared to different forms of MOF/hydrogel structures.[53]

4. Conclusions

A simple and efficient method to the PSM of MOFs, using PEG as a model polymer *via* two different paths is reported. The reaction under UV irradiation showed high efficiency at room temperature. The formation of Zr-MSA-UV2 showed the feasibility of cross-linking the MOF particles with thiol functionalities using difunctional acrylic polymers. There are maybe some side reactions occurred during the UV assisted thiol–ene

click especially when difunctional PEG was used. Reducing the amount of the photo initiator or the UV exposure time could minimize such side reactions. The cross-linked network facilitated the use of MOFs in certain application such as water treatment at industrial level (adsorption of heavy metals and large dye molecules) as the resulting material is processable and non-powder form. The Michael addition pathway had a moderate efficiency but even this low efficiency was enough to render properties such as the colloidal stability in solution. In addition, the phosphine catalyzed Michael reaction evited any side reactions. Both click reactions resulted in efficient grafting of the PEG chains on the surface of the Zr-MSA crystals, leaving certain number of free –SH functionalities (most likely in the core of the Zr-MSA particles) for capturing pollutants. The removal of Hg(II), Cr(VI) and RhB from aqueous solutions using Zr-MSA-UV2 indicated that the pores were still accessible and the free thiol functions were still available to absorb the target species. This simple modification strategy can render processability, flexibility and hydrophilicity to MOF particles while conserving a large part of accessible pores and functionalities. Apart from PEG any other polymer chain or small molecule baring an acrylate functionality could be used to functionalize the MOF particles. The high and rapid adsorption capacity of the resulting material for the removal of the pollutants offer new prospects for the decontamination of water bodies, a matter of great importance for the environment as well as the human health.

Author contributions

The manuscript was written through contributions of all authors. All authors have given approval to the final version of the manuscript.

Data availabibility

The data supporting this article have been included as part of the ESI.†

Conflicts of interest

There are no conflicts to declare.

Acknowledgements

MF acknowledges the financial support of China Scholarship Council (CSC), grant number 201708070001. INC-CNRS is thanked for the post-doctoral fellowship of CM. CM also acknowledges the financial support of Madrid Government under the Multiannual Agreement with Universidad Autónoma de Madrid in the context of the V PRICIT (SI1/PJI/2019–00505). Institut Carnot is also acknowledged for supporting this project. RM acknowledges the financial support of competitive projects of Science and Innovation Ministry of Spain PID2020-114714RB-I00 and Madrid Government S2018/BAA4393.

References

1 H. C. J. Zhou and S. Kitagawa, Metal-Organic Frameworks (MOFs), *Chem. Soc. Rev.*, 2014, **43**(16), 5415–5418, DOI: **10.1039/c4cs90059f**.
2 H. Furukawa, K. E. Cordova, M. O'Keeffe and O. M. Yaghi, The Chemistry and Applications of Metal-Organic Frameworks, *Science*, 2013, **341**(6149), 1230444–1230456, DOI: **10.1126/science.1230444**.
3 N. Stock and S. Biswas, Synthesis of Metal-Organic Frameworks (MOFs): Routes to Various MOF Topologies, Morphologies, and Composites, *Chem. Rev.*, 2012, **112**(2), 933–969, DOI: **10.1021/cr200304e**.
4 M. J. Katz, Z. J. Brown, Y. J. Colón, P. W. Siu, K. A. Scheidt, R. Q. Snurr, J. T. Hupp and O. K. Farha, A Facile Synthesis of UiO-66, UiO-67 and Their Derivatives, *Chem. Commun.*, 2013, **49 (82)**, 9449–9451, DOI: **10.1039/c3cc46105j**.
5 W. Fan, X. Zhang, Z. Kang, X. Liu and D. Sun, Isoreticular Chemistry within Metal–Organic Frameworks for Gas Storage and Separation, *Coord. Chem. Rev.*, 2021, **443**, 213968, DOI: **10.1016/j.ccr.2021.213968**.
6 D. W. Lim, J. Ha, Y. Oruganti and H. R. Moon, Hydrogen Separation and Purification with MOF-Based Materials, *Mater. Chem. Front.*, 2021, **5**(11), 4022–4041, DOI: **10.1039/d1qm00234a**.
7 K. Adil, Y. Belmabkhout, R. S. Pillai, A. Cadiau, P. M. Bhatt, A. H. Assen, G. Maurin and M. Eddaoudi, Gas/Vapour Separation Using Ultra-Microporous Metal-Organic Frameworks: Insights into the Structure/Separation Relationship, *Chem. Soc. Rev.*, 2017, **46**(11), 3402–3430, DOI: **10.1039/c7cs00153c**.
8 B. Van De Voorde, B. Bueken, J. Denayer and D. De Vos, Adsorptive Separation on Metal-Organic Frameworks in the Liquid Phase, *Chem. Soc. Rev.*, 2014, **43**(16), 5766–5788, DOI: **10.1039/c4cs00006d**.
9 B. R. Reiner, N. T. Mucha, A. Rothstein, J. S. Temme, P. Duan, K. Schmidt-Rohr, B. M. Foxman and C. R. Wade, Zirconium Metal-Organic Frameworks Assembled from Pd and Pt PNNNP Pincer Complexes: Synthesis, Postsynthetic Modification, and Lewis Acid Catalysis, *Inorg. Chem.*, 2018, **57**(5), 2663–2672, DOI: **10.1021/acs.inorgchem.7b03063**.
10 P. Q. Liao, J. Q. Shen and J. P. Zhang, Metal–Organic Frameworks for Electrocatalysis, *Coord. Chem. Rev.*, 2018, **373**, 22–48, DOI: **10.1016/j.ccr.2017.09.001**.
11 F. M. Zhang, H. Dong, X. Zhang, X. J. Sun, M. Liu, D. D. Yang, X. Liu and J. Z. Wei, Postsynthetic Modification of ZIF-90 for Potential Targeted Codelivery of Two Anticancer Drugs, *ACS Appl. Mater. Interfaces*, 2017, **9**(32), 27332–27337, DOI: **10.1021/acsami.7b08451**.
12 M. Kubovics, S. Rojas, A. M. López, J. Fraile, P. Horcajada and C. Domingo, Fully Supercritical CO2 Preparation of a Nanostructured MOF Composite with

Application in Cutaneous Drug Delivery, *J. Supercrit. Fluids*, 2021, **178**, 105379, DOI: 10.1016/j.supflu.2021.105379.

13 C. Wang, D. Liu and W. Lin, Metal-Organic Frameworks as a Tunable Platform for Designing Functional Molecular Materials, *J. Am. Chem. Soc.*, 2013, **135**(36), 13222–13234, DOI: 10.1021/ja308229p.

14 S. M. Cohen, Postsynthetic Methods for the Functionalization of Metal-Organic Frameworks, *Chem. Rev.*, 2012, **112**(2), 970–1000, DOI: 10.1021/cr200179u.

15 M. Kim, J. F. Cahill, H. Fei, K. A. Prather and S. M. Cohen, Postsynthetic Ligand and Cation Exchange in Robust Metal-Organic Frameworks, *J. Am. Chem. Soc.*, 2012, 18082–18088, DOI: 10.1021/ja3079219.

16 Z. Wang and S. M. Cohen, Postsynthetic Modification of Metal–Organic Frameworks, *Chem. Soc. Rev.*, 2009, **38**(5), 1315–1329, DOI: 10.1039/b802258p.

17 A. Zimpel, T. Preiß, R. Röder, H. Engelke, M. Ingrisch, M. Peller, J. O. Rädler, E. Wagner, T. Bein, U. Lächelt and S. Wuttke, Imparting Functionality to MOF Nanoparticles by External Surface Selective Covalent Attachment of Polymers, *Chem. Mater.*, 2016, **28**(10), 3318–3326, DOI: 10.1021/acs.chemmater.6b00180.

18 B. Gui, X. Meng, H. Xu and C. Wang, Postsynthetic Modification of Metal-Organic Frameworks through Click Chemistry, *Chin. J. Chem.*, 2016, **34**(2), 186–190, DOI: 10.1002/cjoc.201500621.

19 H. Amer Hamzah, T. S. Crickmore, D. Rixson and A. D. Burrows, Post-Synthetic Modification of Zirconium Metal-Organic Frameworks by Catalyst-Free Aza-Michael Additions, *Dalton Trans.*, 2018, **47**(41), 14491–14496, DOI: 10.1039/c8dt03312a.

20 Y. Goto, H. Sato, S. Shinkai and K. Sada, *Clickable Metal - Organic Framework*. 2008, pp. 14354–14355.

21 W. H. Binder and R. Sachsenhofer, "Click" Chemistry in Polymer and Material Science: An Update, *Macromol. Rapid Commun.*, 2008, **29**(12–13), 952–981, DOI: 10.1002/marc.200800089.

22 C. E. Hoyle, A. B. Lowe and C. N. Bowman, Thiol-Click Chemistry: A Multifaceted Toolbox for Small Molecule and Polymer Synthesis, *Chem. Soc. Rev.*, 2010, **39**(4), 1355–1387, DOI: 10.1039/b901979k.

23 D. P. Nair, M. Podgórski, S. Chatani, T. Gong, W. Xi, C. R. Fenoli and C. N. Bowman, The Thiol-Michael Addition Click Reaction: A Powerful and Widely Used Tool in Materials Chemistry, *Chem. Mater.*, 2014, **26**(1), 724–744, DOI: 10.1021/cm402180t.

24 P. Z. Li, X. J. Wang and Y. Zhao, Click Chemistry as a Versatile Reaction for Construction and Modification of Metal-Organic Frameworks, *Coord. Chem. Rev.*, 2019, **380**, 484–518, DOI: 10.1016/j.ccr.2018.11.006.

25 K. Hindelang, A. Kronast, S. I. Vagin and B. Rieger, Functionalization of Metal-Organic Frameworks through the Postsynthetic Transformation of Olefin Side Groups, *Chem. – Eur. J.*, 2013, **19**(25), 8244–8252, DOI: 10.1002/chem.201300477.

26 B. Gui, G. Hu, T. Zhou and C. Wang, Pore Surface Engineering in a Zirconium Metal-Organic Framework via Thiol-Ene Reaction, *J. Solid State Chem.*, 2015, **223**, 79–83, DOI: 10.1016/j.jssc.2014.06.023.

27 B. Gui, Y. Meng, Y. Xie, J. W. Tian, G. Yu, W. X. Zeng, G. X. Zhang, S. L. Gong, C. L. Yang, D. Q. Zhang and C. Wang, Tuning the Photoinduced Electron Transfer in a Zr-MOF: Toward Solid-State Fluorescent Molecular Switch and Turn-on Sensor, *Adv. Mater.*, 2018, **30**(34), 1–6, DOI: 10.1002/adma.201802329.

28 S. Nayab, V. Trouillet, H. Gliemann, P. G. Weidler, I. Azeem, S. R. Tariq, A. S. Goldmann, C. Barner-Kowollik and B. Yameen, Reversible Diels-Alder and Michael Addition Reactions Enable the Facile Postsynthetic Modification of Metal-Organic Frameworks, *Inorg. Chem.*, 2021, **60** (7), 4397–4409, DOI: 10.1021/acs.inorgchem.0c02492.

29 S. Yang, L. Peng, D. T. Sun, M. Asgari, E. Oveisi, O. Trukhina, S. Bulut, A. Jamali and W. L. Queen, A New Post-Synthetic Polymerization Strategy Makes Metal-Organic Frameworks More Stable, *Chem. Sci.*, 2019, **10**(17), 4542–4549, DOI: 10.1039/c9sc00135b.

30 J. Du, L. Chen, X. Zeng, S. Yu, W. Zhou, L. Tan, L. Dong, C. Zhou and J. Cheng, Hard-and-Soft Integration Strategy for Preparation of Exceptionally Stable Zr(Hf)-UiO-66 via Thiol-Ene Click Chemistry, *ACS Appl. Mater. Interfaces*, 2020, 28576–28585, DOI: 10.1021/acsami.0c10368.

31 N. Mukherjee, A. Das, S. Mukhopadhyay, S. K. Das and T. Jana, Grafting of Polymer Brushes on MOF Surface to Achieve Proton-Conducting Membranes, *ACS Appl. Polym. Mater.*, 2024, **6**(1), 846–858, DOI: 10.1021/acsapm.3c02440.

32 P. Yang, Y. Shu, Q. Zhuang, Y. Li and J. Gu, Metal-Organic Frameworks Bearing Dense Alkyl Thiol for the Efficient Degradation and Concomitant Removal of Toxic Cr(VI), *Langmuir*, 2019, **35**(49), 16226–16233, DOI: 10.1021/acs.langmuir.9b03057.

33 W. L. Jiang, L. G. Ding, B. J. Yao, J. C. Wang, G. J. Chen, Y. A. Li, J. P. Ma, J. Ji, Y. Dong and Y. B. Dong, A MOF-Membrane Based on the Covalent Bonding Driven Assembly of a NMOF with an Organic Oligomer and Its Application in Membrane Reactors, *Chem. Commun.*, 2016, **52**(93), 13564–13567, DOI: 10.1039/C6CC06427B.

34 C. Satheeshkumar, H. J. Yu, H. Park, M. Kim, J. S. Lee and M. Seo, Thiol-Ene Photopolymerization of Vinyl-Functionalized Metal-Organic Frameworks towards Mixed-Matrix Membranes, *J. Mater. Chem. A*, 2018, **6**(44), 21961–21968, DOI: 10.1039/C8TA03803A.

35 K. Knop, R. Hoogenboom, D. Fischer and U. S. Schubert, Poly(Ethylene Glycol) in Drug Delivery: Pros and Cons as Well as Potential Alternatives, *Angew. Chem., Int. Ed.*, 2010, **49**(36), 6288–6308, DOI: 10.1002/anie.200902672.

36 A. Duran, M. Soylak and S. A. Tuncel, Poly(Vinyl Pyridine-Poly Ethylene Glycol Methacrylate-Ethylene Glycol Dimethacrylate) Beads for Heavy Metal Removal, *J. Hazard. Mater.*, 2008, **155**(1–2), 114–120, DOI: 10.1016/j.jhazmat.2007.11.037.

37 K. C. Popat, G. Mor, C. A. Grimes and T. A. Desai, Surface Modification of Nanoporous Alumina Surfaces with Poly (Ethylene Glycol), *Langmuir*, 2004, **20**(19), 8035–8041, DOI: **10.1021/la049075x**.

38 K. Xie, Q. Fu, Y. He, J. Kim, S. J. Goh, E. Nam, G. G. Qiao and P. A. Webley, Synthesis of Well Dispersed Polymer Grafted Metal-Organic Framework Nanoparticles, *Chem. Commun.*, 2015, **51 (85)**, 15566–15569, DOI: **10.1039/c5cc06694h**.

39 C. E. Hoyle and C. N. Bowman, Thiol-Ene Click Chemistry, *Angew. Chem., Int. Ed.*, 2010, **49**(9), 1540–1573, DOI: **10.1002/anie.200903924**.

40 D. Skoog, F. Holler and S. Crouch, *Principles of Instrumental Analysis*, Cengage Learning, 7th edn, 2018.

41 Y. S. Ho, Review of Second-Order Models for Adsorption Systems, *J. Hazard. Mater.*, 2006, **136**(3), 681–690.

42 Z. Hassanzadeh Fard, C. D. Malliakas, J. L. Mertz and M. G. Kanatzidis, Direct Extraction of Ag+ and Hg2+ from Cyanide Complexes and Mode of Binding by the Layered K2MgSn2S6 (KMS-2), *Chem. Mater.*, 2015, **27**(6), 1925–1928, DOI: **10.1021/acs.chemmater.5b00374**.

43 A. Farrukh, A. Akram, A. Ghaffar, S. Hanif, A. Hamid, H. Duran and B. Yameen, Design of Polymer-Brush-Grafted Magnetic Nanoparticles for Highly Efficient Water Remediation, *ACS Appl. Mater. Interfaces*, 2013, **5**(9), 3784–3793, DOI: **10.1021/am400427n**.

44 G. Kumar and D. T. Masram, Sustainable Synthesis of MOF-5@GO Nanocomposites for Efficient Removal of Rhodamine B from Water, *ACS Omega*, 2021, **6**(14), 9587–9599, DOI: **10.1021/acsomega.1c00143**.

45 G. Dong, Spectrophotometric Study on Kinetics and Thermodynamics of Adsorption and Catalytic Transformation of K2Cr2O7 to K2CrO4 by Natural Hermit Crab Shell Powder, *Chem. Sci. J.*, 2011, **2**, 1–9, DOI: **10.4172/2150-3494.1000030**.

46 P. Yang, Y. Shu, Q. Zhuang, Y. Li and J. Gu, A Robust MOF-Based Trap with High-Density Active Alkyl Thiol for the Super-Efficient Capture of Mercury, *Chem. Commun.*, 2019, **55**(86), 12972–12975, DOI: **10.1039/c9cc06255f**.

47 J. He, K. K. Yee, Z. Xu, M. Zeller, A. D. Hunter, S. S. Y. Chui and C. M. Che, Thioether Side Chains Improve the Stability, Fluorescence, and Metal Uptake of a Metal-Organic Framework, *Chem. Mater.*, 2011, **23**(11), 2940–2947, DOI: **10.1021/cm200557e**.

48 G. J. Grant, K. E. Rogers, W. N. Setzer and D. G. VanDerveer, Crown Thioether Complexes of Trivalent Transition Metal Ions. The Crystal Structure of [Cr(18S6) Cl3], *Inorg. Chim. Acta*, 1995, **234**(1–2), 35–45, DOI: **10.1016/0020-1693(95)04462-I**.

49 X. Wang, Z. Dai, X. Zhou, H. Chen, Y. Cao, J. Hou and X. Wang, Recyclable Thiol-Modified Zr-Based MOFs/Hydrogel Composite Beads for Effective Removal of Hg(II), *Prog. Nat. Sci.:Mater. Int.*, 2023, **33**(5), 644–651, DOI: **10.1016/j.pnsc.2023.11.009**.

50 L. Wang, H. Xu, J. Gao, J. Yao and Q. Zhang, Recent Progress in Metal-Organic Frameworks-Based Hydrogels and Aerogels and Their Applications, *Coord. Chem. Rev.*, 2019, **398**, 213016, DOI: **10.1016/j.ccr.2019.213016**.

51 H. Laddha, N. B. Jadhav, M. Agarwal and R. Gupta, Enumeration of Research Journey of MOF@hydrogel Composite Beads as Potential Adsorbents for Adsorptive Elimination of Toxic Contaminants, *J. Environ. Chem. Eng.*, 2023, **11**(5), 110642, DOI: **10.1016/j.jece.2023.110642**Elsevier Ltd.

52 S. Daradmare, M. Xia, V. N. Le, J. Kim and B. J. Park, Metal–Organic Frameworks/Alginate Composite Beads as Effective Adsorbents for the Removal of Hexavalent Chromium from Aqueous Solution, *Chemosphere*, 2021, **270**, 129487, DOI: **10.1016/j.chemosphere.2020.129487**.

53 H. Zhu, Q. Zhang and S. Zhu, Alginate Hydrogel: A Shapeable and Versatile Platform for in Situ Preparation of Metal–Organic Framework–Polymer Composites, *ACS Appl. Mater. Interfaces*, 2016, **8**(27), 17395–17401, DOI: **10.1021/acsami.6b04505**.